1   **Atmospheric transport and deposition of microplastics in a remote mountain catchment**

2   Steve Allen[† a,b], Deonie Allen[†*a], Vernon R. Phoenix[b], Gaël Le Roux[a], Pilar Durantez[a], Anaëlle

3   Simonneau[c], Stéphane Binet[a,c], Didier Galop[d]

4

5   [a] EcoLab (Laboratoire Ecologie Fonctionnelle et Environnement), ENSAT, UMR-CNRS 5245,

6   Castanet Tolosan (France)

7   [b] Department of Civil and Environmental Engineering, University of Strathclyde, Glasgow, G1

8   1XQ, Scotland, UK

9   [c] ISTO, CNRS UMR 7327, Université d'Orléans, BRGM (France)

10   [d] GEODE, UMR-CNRS 5602, Université Toulouse Jean Jaurès (France)

11   [†] joint first authors (S Allen: https://orcid.org/0000-0002-2333-6514; D Allen:

12   https://orcid.org/0000-0002-4038-9394)

13   [*] corresponding author: deonie.allen@ensat.fr; deoniea@gmail.com

14

15   **Abstract**

16   Plastic litter is an ever-increasing global issue and one of this generation's key environmental

17   challenges. Microplastics have reached oceans via river transport on a global scale, but

18   outside two mega-cities, Paris (France) and Dongguan (China), there is a lack of information

19   on atmospheric microplastic deposition or transport. Here we present the observations of

20   atmospheric microplastic deposition in a remote, pristine, mountain catchment (French

21   Pyrenees). We analyse five months of samples representing atmospheric wet and dry

22   deposition and identify fibres up to ~750 μm long and fragments ≤300μm as microplastics.

23   We document relative daily counts of 249 fragments, 73 films and 44 fibres per square

24   metre depositing on the catchment. Air mass trajectory analysis shows microplastic

25   transport through the atmosphere over a distance of up to 95km. We suggest that

26   microplastics can reach and affect remote, sparsely inhabited areas through atmospheric

27   transport.

28   Key words: microplastic, atmospheric fallout, aerosol plastic, remote area.

29   **Main text**

30   Plastic industry experts estimate global manufacture of 335 million tonnes (Mt) of plastic in

31   2016[1]. Of the 335Mt worldwide, 60Mt was produced in Europe, of which ~40% is packaging

32   (short-term or single use). However, in 2016 27.1Mt was recovered as waste for recycling,

33   energy recovery (burning) or placed in landfill[2,3]. Some plastics remain in service for up to 50

34   years, which helps explain some of the 32.9Mt discrepancy in the plastics mass balance.

35   While plastic is recognised to biodegrade very slowly, degradation to micro (5mm-1µm) and

36   nanoplastics (<1µm) does occur[4,5]. Thus, plastic waste can start as macroplastic pieces

37   (bottles, packaging etc.) and over time degrades to microplastic (MP) particles or smaller.

38   Mattson et al.[6] estimate 10% of created plastics enter the ocean annually, accounting for a

39   portion of the 32.9Mt plastics waste. However, this highlights questions on the fate of the

40   remaining plastic. Large amounts of macroplastic waste would be noticed in the terrestrial

41   environment, but if this waste was degraded to micro-sized particles it could evade easy

42   detection. Recent studies have identified MP on alpine river floodplains[7] and lake sediment[8]

43   illustrating terrestrial MP occurrence, and in mega-cites as aerosol pollution[9–12]. The recent

44   research on atmospheric fallout in Paris (France)[9–11] and Dongguan (China)[12] suggests

45   atmospheric MP conveyance and corresponding deposition. Soil/sediment/lake samples

46   provide an informative terrain-based analysis of plastic[7,13–16] occurrence however

47   determination of atmospheric MP beyond intra-city deposition requires source specific and

48   remote atmospheric sampling.

49   This research provides unequivocal evidence of direct atmospheric fallout of MP in a remote

50   area of the Pyrenees Mountains. The Pyrenees mountainous regions are anecdotally

51   considered pristine wilderness due to limited development, difficulty of human access and

52   distance from major populations or industrial centres. The study site is located at the

53   Bernadouze meteorological station[17], 42°48'14.6"N 1°25'06.8"E and 1425m a.s.l., within the

54   Vicdessos catchment and Mid-Pyrenees mountains in south-west of France (Supplementary

55   Note 1 - Detailed site description). The local vicinity is sparsely populated, without industrial,

56   commercial or large agricultural activities and is primarily used for recreational activities

57   (hiking, skiing, environmental education and scientific research). The closest local residential

58   area is a village ~6km to the south-east (Vicdessos village, population ~540[18]) with a

59   moderately sized town located ~25km to the north-east (Foix, population ~9,720[18]).

60   The presented research considers five months of atmospheric deposition collected from the

61   field site. Five samples of total atmospheric deposition (wet and dry), from two separate

62   monitoring devices, were analysed to identify if MPs are present in the remote mountain

63   catchment. Regular (monthly) sampling campaigns were proposed, however weather

64   conditions restricted site access resulting in irregular monitoring intervals (Methodology,

65   Supplementary Table 1). The objective in observing the case study atmospheric deposition

66   was to identify (1) if MPs are present in atmospheric fallout in this remote mountainous

67   location and (2) if MP are present, in what quantity, size, shape and plastic type do they

68   occur? The purpose of this study was to take steps towards discovering the extent of MP

69   atmospheric deposition in remote terrestrial locations.

70 **MP particles in the remote mountain catchment**

71 MP fragments, fibres and films were found, and confirmed (through visual microscopy

72 inspection and µRaman analysis[19]) in all atmospheric deposition samples collected from the

73 field site. This illustrates that for this location there is an atmospheric MP presence. The

74 atmospheric MP deposition captured in the collectors are presented in Figure 1.

75 Figure 1 near here

76 Details of local meteorological conditions recorded at the sampling site are provided in

77 Supplementary Table 1 in conjunction with normalised MP counts ($MP/m^2/day$) per day. The

78 meteorological record illustrates lower relative precipitation and fewer storms (rain or snow)

79 in November compared to the following months. The relative snowfall increased over the

80 monitoring period while rainfall was greatest in the January. Monthly average wind speed

81 fluctuated around 1.1(±0.6)m/s with a maximum recorded wind speed of 7.1m/s in

82 December. December-March illustrate wind speeds >4m/s and the greatest relative number

83 of wind events (>2m/s and >3m/s) occurred in March. The number of >1m/s events were

84 greatest in November and March, declining to the lowest frequency in February.

85 Field sample MP counts illustrate an average daily particle deposition of $365/m^2/day$ (±69,

86 standard deviation). Sample MP counts were normalised to represent daily atmospheric

87 deposition ($MP/m^2/day$) as site access limitations resulted in inconsistent monitoring

88 durations (November extended 12 days, December 19 days, January and March 34 days,

89 February 41 days).

90 Both rainfall and snowfall show moderate to strong significant correlations with MP count in

91 the original dataset ($r \geq 0.8$, $p < 0.05$) and to the monitoring duration (days) (Supplementary

92 Note 2). The normalised dataset presents a positive correlation to the frequency of wind

93   speeds >1m/s (light air-strong wind movement) (r>0.8, p<0.05) suggesting MP transport and

94   deposition may be influenced by wind movement. The maximum rainfall intensity also

95   presents a strong positive correlation (r>0.9, p <0.05) suggesting that individual events and

96   the intensity of events may influence atmospheric MP deposition (scavenging)[20]. While it is

97   acknowledged that the dataset is limited, the number of snowfall events also shows a

98   positive correlation with normalised MP deposition (r≥0.6, p<0.05). The duration (average

99   and maximum) of both rainfall and snowfall events illustrate negative correlations with MP

100   deposition (r≤-0.6) suggesting event occurrence and intensity rather than duration may

101   positively influence MP deposition[21,22]. Despite long durations (≤41 days) represented by the

102   samples, this preliminary dataset suggests that rain, snow and wind events may be drivers in

103   MP deposition at this site. This supports the suggestion by Dris et al.[10] that precipitation

104   events may be a positive driver in atmospheric MP fallout.

105   The samples collected for the January – March monitoring period contained a visible

106   quantity of orange quartz-like fine dust. This dust presented size (d50 ~8μm), colour and

107   indicative chemical signature descriptive of Saharan dust[23,24] (further details in

108   Supplementary Data). The fine dust, and other particulate matter potentially including some

109   MP particles, are possibly Saharan, North Africa or Iberic sourced material (or potentially

110   sourced along this trajectory)[25]. For example, long-range transport of dust has been shown

111   by van der Does et al.[26] findings of ultra-giant particles (<400μm) traveling trans-oceanic up

112   to 3,500km. The distance MP can travel is currently unknown and further event–based

113   research is needed to identify source and transport vectors of atmospheric MP particles.

114   **Characteristics of MP particles**

115   Characterisation was completed following the identification guide presented by Hidalgo-Ruz

116   et al. and Noren et al.[27,28] in conjunction with µRaman analysis. MP particle size or length

117   was defined using the particle characterisation and count functions in ImageJ/FIJI[29],

118   following the method presented by Erni-Cassola et al.[30]. The overall particle size for MP

119   particles are presented in Figure 2, with individual monitoring period sample fragment sizes

120   illustrated in Figure 2b.

121   Figure 2 near here

122   The majority of environmental MP studies that have considered particle size distribution

123   (PSD) illustrate an increasing trend in the number of finer fragments (significantly greater

124   number of MP fragments with smaller particle size)[9,12,31]. The remote atmospheric

125   deposition samples illustrate the majority of identified MP fragments to fall ≤50µm and the

126   overall fragment size trend to follow previous MP particle size trends. When considered

127   relative to the monitoring period (Figure 2b) there is a slight shift in PSD curve that appears

128   to correspond to the fine dust deposition. Samples with no visible quantity of fine dust

129   (November, December) show a greater quantity of smaller fragments. The fine dust laden

130   samples show a small increase in primary fragment size (February-March). It is noted that for

131   the fine dust sample periods there are a greater number of elevated wind periods (wind

132   events >2m/s and greater), higher maximum recorded wind speeds and interspersed periods

133   of calm (wind speed <0.5m/s) that may assist in the conveyance and deposition of the MP

134   fragments.

135   The length of plastic fibres found in the atmospheric fallout samples (Figure 2c) suggests the

136   predominant fibre lengths to be 100-200µm and 200-300µm. Cai et al.[12] found the majority

137   of fibres in Dongguan to be 200-700µm in length with fibres of ≥4200µm (longest fibre),

138   while Dris et al.[10,11] primarily found fibres of 200-600µm, with the longest recorded fibre

139   ~5000µm. When the scale for fibre length analysis is modified to fit previous studies, the

140   Pyrenees site fibre lengths fall predominantly between 200-700µm (47%) (Cai et al.[12]

141   present~30% in this predominant category) and 50-200µm (30%) (Dris et al.[10,11] illustrate a

142   higher predominant fibre length of 400-600µm, ~23%). The longest fibre identified as a

143   plastic fibre in this mountain field study was 3000µm. Film size has not specifically been

144   evaluated in previous atmospheric MP analysis so limited comparative information is

145   currently available. Films can be very thin, flat and therefore provide a greater surface area

146   for atmospheric conveyance relative to a fragment of the same mass (Figure 2a and 2d).

147   Within this mountain field study, the predominant film diameter was 50-200µm, larger than

148   the predominant fragment size.

149   Raman spectroscopic analysis provides a verification of fragments, fibres and films as

150   plastic[31] and characterisation of plastic type (Figure 1). The predominant plastic found in the

151   samples is polystyrene (PS) (as fragments), closely followed by polyethylene (PE). PS and PE

152   are used in many single use plastic items and in packaging material. Approximately 40% of

153   plastic demand is for plastic packaging and PS or PE products[32]. PS and PE are recyclable

154   products, however the European recycling rate is currently ~31% overall (all plastics)

155   and ~41% for plastic packaging (2016[32]) with 3.4Mt of plastic packaging disposed in EU

156   landfill. PE has a low density compared to other plastics, 0.92-0.97g/cm[27] and is a common

157   film plastic (including plastic bags)[33]. PS is a common packaging material having thermal

158   insulating features and the ability to provide both strong and light weight plastic products.

159   PS has a higher density than PE, 0.96-1.1g/cm^{3},[27] however it is often used in a foam form for

160   packaging, insulation and protection, resulting is a significantly lowered density.

161   Polypropylene (PP) comprises 18% of the identified plastic particles (fibres primarily PP and

162 PET). PP is used in packaging, textiles and re-usable products. It is the least dense of all

163 plastics (0.9-0.91g/cm^3)[27] and due to its use in textile industry is constructed as fibres as well

164 as objects or films.

165 The composition of plastic fallout varies over the monitoring period. Initial correlation

166 analysis does not indicate any strong, significant correlations between plastic type and

167 recorded meteorology (rainfall, snowfall, wind speed or events). The complexity of the

168 plastic composition may be due to the source of plastic particles (and therefore wind

169 direction, wind strength), the occurrence of storm events and the duration of calm days

170 relative to event occurrence. The initial consideration of atmospheric MP fallout to

171 meteorological conditions does not suggest a simple meteorological mechanism driving

172 specific or preferential plastic deposition at this field site but does illustrate PS, PE and PP to

173 be the three greatest contributors to the atmospheric fallout at this location.

174 **Remote MP deposition compared to mega-city MP**

175 The MP deposition recorded at this field site equates to an average daily MP deposition of

176 365/m^2/day (±69, particles ≥ 5μm). Previous atmospheric fallout monitoring[11,12] undertaken

177 in high density urban areas identified daily fallout of 110(±96) and 53(±38) particles/m^2/day

178 (Paris)[10,34] and 228(±43) particles/m^2/day (36 MP particles/m^2/day confirmed) (Dongguan)[12].

179 Both the Paris and Dongguan studies counted and analysed particles ≥100μm, ≥50 μm and

180 ≥200μm respectively. If only ≥200μm particles are counted in the remote mountain field

181 samples, this equates to 40(±20) particles/m^2/day, 70% as fibres. The Pyrenees field site MP

182 deposition is comparable to the reported mega-city and suburban atmospheric MP

183 deposition despite the remote and mountainous location of notable distance from urban city

184 development or infrastructure.

185   Both the Paris and Dongguan studies primarily focused on MP fibres. If only fibres are

186   considered, the relative daily MP fibre deposition is 36(±18)fibres/m^2/day ≥100μm, or

187   28(±13)fibres/m^2/day ≥200μm. This is lower but comparable to mega-city average MP

188   counts. The fibre count for the Pyrenean site for MP fibres ≥100μm ranges from 22-62

189   fibres/m^2/day. The Paris mega-city study includes periods of lower MP deposition than seen

190   in this field study (Paris MP deposition range 2-355 MP/m^2/day) potentially due to the

191   greater precipitation quantity and frequency at the Pyrenees field site compared to the Paris

192   study period. It is noted that, in concurrence with the Paris and Dongguan findings, there

193   appears to be no direct correlation between MP deposition and average daily rainfall but

194   that the occurrence of precipitation events (rain or snow) and their specific characteristics,

195   intensity and frequency, may be drivers in atmospheric fallout.

196   The Paris and Dongguan studies MP sample composition differs in plastic type as well as

197   shape to this study's findings. PS and PE form a large portion of the plastic type found in the

198   Pyrenees field site. The majority of PS particles were fragments while most fibres were PET

199   or PP. The Pyrenees field study, similarly to the Swiss floodplain findings[7] found MP

200   composition to differ from the city atmospheric findings[11,12]. While acknowledging the

201   different environmental compartment, there have also been several oceanic focused studies

202   that identified high counts of PS alongside PE and PP[35]. Emerging research on the

203   degradation rate of plastics by type suggest that PS, especially EPS, is highly sensitive to

204   mechanical and UV degradation (when compared to PP and PE)[4]. Expanded PS microplastics

205   may be less dense and more easily entrained (therefore transported), and this may help

206   explain the findings at this field site. The composition of plastic waste lost to the

207   environment (not recycled or recovered) is not well documented and this, combined with

208   limited knowledge on degradation rates makes establishing the plastic waste type, shape

209   and size 'escaping' to the environment difficult to quantify or characterise.

210   **Remote atmospheric MP source and transport analysis**

211   Atmospheric MP source and transport analyses are new to MP research. Local to regional

212   transport has been considered for this field site using two methods, a simple MP settling

213   calculation and short-duration Hysplit4 back-trajectory modelling (see Methodology). Back-

214   trajectory duration is defined as ~2hrs (0.1m/s settling velocity[36] for 600m a.g.l. Pyrenean

215   planetary boundary layer depth(PBL)[37]) and each individual wind (>2m/s), rain and snow

216   event has been analysed to provide a spatial context for local MP transport. The simple MP

217   settling calculations, using MP settling velocity, event wind speed and direction and PBL

218   depth[37], provide basic, linear back-trajectories for MP deposited at the field site due to initial

219   entrainment or uplift and horizontal (wind) conveyance (without further mechanical or

220   convective lift). The MP source area or zone of influence defined by this method extends

221   28km north-west to south-west, along the sparsely populated Aulus-les-Bains, Ercé and

222   Massat valleys, over the Guzet-Neige ski fields and south-east along the Vicdessos valley

223   (Figure 3a-b). Wind events >2m/s illustrate a local MP source area across Aulus-les-Bains and

224   the Saint-Girons valleys (42km to the north-west) and 20km to the north-east over Tarascon-

225   sur-Ariège (village populations <6000).

226   Figure 3 near here

227   Hysplit4 back-trajectory modelling allows individual event air parcels to be back-traced

228   illustrating the air parcel trajectory. Using the calculated back-trajectory duration (see

229   Methodology), models for individual rain, snow and wind events were created and collated

230   to provide event-based back-trajectory frequency maps (Figure 3c-e). These short duration

231   back-trajectories include localised updraft, convective mixing and advection, thus extending

232   the MP transport trajectories and the source area 60km to the east, 75km to the west and

233   south and 95km to the north of the site. Hysplit4 MP source areas extend into western

234   Andorra (Andorra le Vella, population ~22,250), the Spanish Pyrenees, the Saint Gaudens

235   valley, across Foix to Muret (population~24,975). However, like the MP settling calculations,

236   they still fall short of the more densely populated and industrialised areas likely to be

237   significant MP emission sources (Toulouse (population ~466,000), Barcelona (population

238   1.6million), Zaragoza (population ~661,000). This dataset does not support long-range

239   transport analysis due to the sampling time-step, however MP emissions are unlikely to be

240   limited to local sources (<100km) due to low local population density.

241   **Evidencing remote atmospheric deposition and transport**

242   This study reports atmospheric deposition of MP in a remote Pyrenean mountain location.

243   The research shows the monitored site received large numbers of MP particles (365 MP

244   particles/m^2/day) in atmospheric deposition collectors over the winter period of 2017-2018.

245   The presented research illustrates the presence of MP in non-urban atmospheric fallout.

246   Analysis for this single site suggests a tentative but possibly important link between

247   precipitation (rain and/or snow), wind speed and direction to MP deposition. Initial local MP

248   trajectory assessment indicates an MP source area extending to 95km from the site,

249   reaching several towns (populations <25,000) but not the city MP emission sources such as

250   Toulouse or Zaragoza. The data cannot prove long-range transport, however air mass

251   trajectory, MP transport and settling considerations suggest MP emission sources to at least

252   be regional (>100km) given the population density within this local area. Longer-distance

253   transport modelling may be possible but requires event specific sampling and back-

254 trajectory analysis to identify the extent of this transport. It is highly recommended that

255 further monitoring and analysis be undertaken using separate dry and wet deposition

256 sampling equipment. This would advance the understanding of precipitation influence on

257 atmospheric MP deposition and wind trajectory impact on quantity and composition of

258 atmospheric MP fallout.

259

260 **Data availability**. The authors confirm that all data underlying the results presented in this

261 study are available within the Supplementary Information files and can be downloaded in

262 conjunction with this paper.

263 **References**

264 1.   Rosevelt, C., Los Huertos, M., Garza, C. & Nevins, H. M. Marine debris in central

265   California: Quantifying type and abundance of beach litter in Monterey Bay, CA. *Mar.*

266   *Pollut. Bull.* **71**, 299–306 (2013).

267 2.   PlasticsEurope. *Plastics – the Facts 2014 / 2015 An analysis of European plastics*

268   *production , demand and waste data*. (Plastic Recycling and Recovery Organisations

269   (EPRO), 2015).

270 3.   PlasticsEurope. *Plastics – the Facts 2017, An analysis of the European plastics*

271   *production, demand and waste data*. (PlasticsEurope, European Association of Plastics

272   Recycling and Recovery Organisations, 2017).

273 4.   Song, Y. K. *et al.* Combined Effects of UV Exposure Duration and Mechanical Abrasion

274   on Microplastic Fragmentation by Polymer Type. *Environ. Sci. Technol.* **51**, 4368–4376

275   (2017).

276   5.   da Costa, J. P. Micro- and nanoplastics in the environment: Research and

277   policymaking. *Curr. Opin. Environ. Sci. Heal.* **1**, 12–16 (2018).

278   6.   Mattsson, K., Hansson, L.-A. & Cedervall, T. Nano-plastics in the aquatic environment.

279   *Environ. Sci. Process. Impacts* **17**, 1712–1721 (2015).

280   7.   Scheurer, M. & Bigalke, M. Microplastics in Swiss floodplain soils Microplastics in

281   Swiss floodplain soils. (2018). doi:10.1021/acs.est.7b06003

282   8.   Hurley, R., Woodward, J. & Rothwell, J. J. Microplastic contamination of river beds

283   significantly reduced by catchment-wide flooding. *Nat. Geosci.* **11**, 251–257 (2018).

284   9.   Gasperi, J. *et al.* Microplastics in air: Are we breathing it in? *Curr. Opin. Environ. Sci.*

285   *Heal.* **1**, 1–5 (2018).

286   10.   Dris, R. *et al.* A first overview of textile fibers, including microplastics, in indoor and

287   outdoor environments. *Environ. Pollut.* **221**, 453–458 (2017).

288   11.   Dris, R., Gasperi, J., Saad, M., Mirande, C. & Tassin, B. Synthetic fibers in atmospheric

289   fallout: A source of microplastics in the environment? *Mar. Pollut. Bull.* **104**, 290–293

290   (2016).

291   12.   Cai, L. *et al.* Characteristic of microplastics in the atmospheric fallout from Dongguan

292   city, China: preliminary research and first evidence. *Environ. Sci. Pollut. Res.* **24**,

293   24928–24935 (2017).

294   13.   Corcoran, P. L. Environmental Science Processes & Impacts Benthic plastic debris in

295   marine and fresh water environments. *Environ. Sci. Process. Impacts* **17**, 1363–1369

296   (2015).

297   14.   Zbyszewski, M., Corcoran, P. L. & Hockin, A. Comparison of the distribution and

298   degradation of plastic debris along shorelines of the Great Lakes , North America. *J.*

299   *Great Lakes Res.* **40**, 288–299 (2014).

300   15.   Zhang, K. *et al.* Microplastic pollution of lakeshore sediments from remote lakes in

301   Tibet plateau, China. *Environ. Pollut.* **219**, 450–455 (2016).

302   16.   Watkins, L., McGrattan, S., Sullivan, P. J. & Walter, M. T. The effect of dams on river

303   transport of microplastic pollution. *Sci. Total Environ.* (2019).

304   doi:https://doi.org/10.1016/j.scitotenv.2019.02.028

305   17.   Centre d'Etudes Spatiales de la BIOsphere (CESBIO). Donnees meteorologiques – Sud

306   Ouest Bernadouze. (2018). Available at: http://www.cesbio.ups-

307   tlse.fr/data_meteo/index.php?perma=1319145390.

308   18.   INSEE. Institut national de la statistique et des etudes economiques. (2018). Available

309   at: https://www.insee.fr/fr/statistiques/3293086?geo=COM-09334. (Accessed: 24th

310   June 2018)

311   19.   Araujo, C. F., Nolasco, M. M., Ribeiro, A. M. P. & Ribeiro-Claro, P. J. A. Identification of

312   microplastics using Raman spectroscopy: latest developments and future prospects.

313   *Water Res.* **142**, 426–440 (2018).

314   20.   Zwaaftink, C. D. G. *et al.* Temporal and spatial variability of Icelandic dust emissions

315   and atmospheric transport. *Atmos. Chem. Phys.* 10865–10878 (2017).

316   doi:10.5194/acp-17-10865-2017

317   21.   Camarero, L., Bacardit, M., de Diego, A. & Arana, G. Decadal trends in atmospheric

318   deposition in a high elevation station: Effects of climate and pollution on the long-

319   range flux of metals and trace elements over SW Europe. *Atmos. Environ.* **167**, 542–

320   552 (2017).

321   22.   Marticorena, B. *et al.* Mineral dust over west and central Sahel: Seasonal patterns of

322   dry and wet deposition fluxes from a pluriannual sampling (2006-2012). *J. Geophys.*

323   *Res. Atmos.* **122**, 1338–1364 (2017).

324   23.   Morales-Baquero, R., Pulido-Villen, E. & Reche, I. Chemical signature of Saharan dust

325   on dry and wet atmospheric deposition in the south-western Mediterranean region.

326   *Tellus Ser. B* **1**, 1–12 (2013).

327   24.   Schwikowski, M., Seibert, P., Baltensperger, U. & Gaggeler, H. W. A study of an

328   outstanding Saharan dust event at the high-alpine site Jungfraujoch, Switzerland.

329   *Atmos. Environ.* **29**, 1829–1842 (1995).

330   25.   Dessens, J. & Van Dinh, P. Frequent Saharan Dust Outbreaks North of the Pyrenees: A

331   sign of a climatic change? *Weather* **45**, 327–333 (1990).

332   26.   van der Does, M., Knippertz, P., Zschenderlein, P., Giles Harrison, R. & Stuut, J.-B. W.

333   The mysterious long-range transport of giant mineral dust particles. *Sci. Adv.* **4**,

334   (2018).

335   27.   Hidalgo-Ruz, V., Gutow, L., Thompson, R. C. & Thiel, M. Microplastics in the marine

336   environment: A review of the methods used for identification and quantification.

337   *Environ. Sci. Technol.* **46**, 3060–3075 (2012).

338   28.   Noren, F. *Small plastic particles in Coastal Swedish waters*. *N-Research, KIMO Sweden*

339   (2007).

340   29.   Schindelin, J. *et al.* Fiji: an open-source platform for biological image analysis. *Nat.*

341   *Methods* **9**, 676–682 (2012).

342   30.   Erni-Cassola, G., Gibson, M. I., Thompson, R. C. & Christie-Oleza, J. A. Lost, but Found

343   with Nile Red: A Novel Method for Detecting and Quantifying Small Microplastics (1

344   mm to 20 μm) in Environmental Samples. *Environ. Sci. Technol.* **51**, 13641–13648

345   (2017).

346   31.   Schymanski, D., Goldbeck, C., Humpf, H. U. & Fürst, P. Analysis of microplastics in

347   water by micro-Raman spectroscopy: Release of plastic particles from different

348   packaging into mineral water. *Water Res.* **129**, 154–162 (2018).

349   32.   European Comission. A European Strategy for Plastics in a Circular Economy. *Eur. Com.*

350   24 (2018). doi:10.1021/acs.est.7b02368

351   33.   Magnusson, K. *et al.* Swedish sources and pathways for microplastics to the marine

352   environment. A review of existing data. *IVL Rep.* 1–89 (2016).

353   34.   Dris, R. *et al.* Beyond the ocean: Contamination of freshwater ecosystems with (micro-

354   ) plastic particles. *Environ. Chem.* **12**, 539–550 (2015).

355   35.   Shim, W. J., Hong, S. H. & Eo, S. Chapter 1 - Marine Microplastics: Abundance,

356   Distribution, and Composition. in *Microplastic Contamination in Aquatic Environments*

357   (ed. Zeng, E. Y.) 1–26 (Elsevier, 2018). doi:https://doi.org/10.1016/B978-0-12-813747-

358   5.00001-1

359   36.   Zender, C. S. Mineral Dust Entrainment and Deposition (DEAD) model: Description and

360   1990s dust climatology. *J. Geophys. Res.* **108**, 4416 (2003).

361   37.   Sanchez, E., Yague, C. & Gazetner, M. A. Planetary boundary layer energetics

362   simulated from a regional climate model over Europe for present climate and climate

363   change conditions. *Geophys. Res. Lett.* **34**, (2007).

Author contributions

376   SA and DA designed the study, undertook all analysis and co-authored the manuscript. GLR

377   and VRF provided study design and analytical guidance and assisted preparation and revision

378   of the manuscript. PD undertook all field sampling and field protocol design, assisted in

379   sample preparation and contributed to the manuscript. AS, SB and DG provided financial

380   support and field site access that enabled this study to occur and contributed to the

381   manuscript.

382   **Corresponding Author**: The corresponding author for correspondence and requests for

383   materials relating to this paper is Dr D Allen, deonie.allen@ensat.fr.

384   **Competing interests**: The authors declare no competing interests.

385   **Figure Cations**

386   Figure 1. MP occurrence, MP type, recorded local rain and snow fall for the monitored period, wind

387   speed and wind events. See supplementary information for comment on the fragment, fibre and film

388   ratio. The types of plastics found in the atmospheric fallout derived from Raman spectroscopy

389   analysis, SpectraGryph[©] spectral analysis software and libraries[44-48]. The plastic types are presented

390   as abbreviations: PS (polystyrene); PE (polyethylene); PP (polypropylene); PVC (polyvinyl chloride);

391   PET (polyethylene terephthalate); other (uncharacterised).

392   Figure 2. Deposited MP characterisation. (a) and (b) illustrate the particle size distribution for the MP

393   particles identified in the monitoring period. (c) illustrates the range and predominant fibre lengths.

394   (d) illustrates the average diameter of films collected in the rain and snow collectors during the

395   monitoring periods

396   Figure 3. MP transport trajectories relative to recorded meteorology (simplistic MP settling velocity

397   trajectory calculation, Methodology Eqn.4) and Hysplit4 back-trajectory modelling. Figure 3a

398   illustrates the rain (n=165) and snow (n=186) event trajectories calculated from the maximum

399   recorded wind speed and wind direction of each storm. Figure 3b illustrates the trajectories of wind

400   events >2m/s (n=197). Figure 3c-e present the Hysplit4 back-trajectory model results for each

401   individual rain, snow or wind event >2m/s. The results have been collated and are presented as

402   trajectory frequency graphs. The wind direction data is presented in reference to local populated

403   areas to provide spatial reference.

404

Methods

Field sampling and data collation

The field site meteorology and sample station was visited five (5) times over the five (5) month monitoring period for acquisition of samples from atmospheric fallout collectors. The sampling period extended over 2017-2018 from November to March. Samples were ideally collected every 4 weeks but due to climatic conditions restricting access the sample periods for the five samples were inconsistent (sample durations: 12, 19, 34, 41 and 34 days respectively for samples November to March). Field blanks were also collected. During this period two independent atmospheric deposition collectors were active at the site. The first collector was a Palmex Rain Sampler (RS1) with a sampling area of $0.014m^2$ (dia. 135mm) (constructed of UV resistant PVC and stainless steel). The second collector installed and sampled from was a NILU Particulate Fallout Collector (p.n.o 9721) with a sampling area of $0.03m^2$ (dia. 200mm) (constructed of HDPE and stainless steel). Both collectors were open to the atmosphere for the total period of sampling therefore all samples are a combination of dry and wet atmospheric fallout. The samples collected from each atmospheric fallout collector were kept separate (both during field sampling and laboratory sample preparation) thus providing a duplicate sample dataset for each monitoring period.

During collection of the sample material (and all times when near the sampler) all persons were careful to remain down-wind of the sampler, samples exposure time was kept to a minimum and wherever possible cotton clothing was worn to minimise contamination. The total sample volume was collected (without subsampling). Samples from the Palmex collector were decanted into clean glass 2L bottles in the field capped and transported back to the laboratory. The field sample container from the NILU collector was capped and transported back to the laboratory where samples were decanted into clean glass 2L bottles in the laboratory 'clean room'. All decanted samples were stored in a dark walk-in refrigerator (at 4 deg C) until filtration and sample processing commenced.

429   In conjunction with physical atmospheric samples wind, humidity, temperature, rainfall and snowfall

430   data was recorded at the monitoring site by the CESBIO meteorological gauging station [17]. This

431   dataset provided local microclimate information at a 30 minute time-step.

432   **Sample processing preparation for MP analysis**

433   All samples (2 x 5 field samples) contained varying amounts of organic and inorganic matter including

434   biofilm and dust. To aid analysis it is necessary to remove as much of the biogenic and non-plastic

435   inorganic material as possible without damaging or losing potential plastic particles. It is also

436   necessary to remove biofilm from the plastic prior to μRaman spectroscopy to ensure effective

437   analysis (spectra clarity). To this end, protocols were selected with the minimum physical

438   manipulation, least number of steps and the least aggressive digestion chemicals and temperatures

439   possible whist achieving the desired results. Sample material was filtered through a 0.45μm PTFE

440   47mm diameter membrane (Whatman) using borosilicate laboratory glass filtration equipment and

441   vacuum dried with ethanol (96%.vol). Filters were examined and photographed under a stereo

442   microscope Olympus SZX10 with an Olympus SC30 camera attachment (and visually checked using an

443   Axiostar Plus (x50) microscope) to record as much detail of potential plastic particles as possible prior

444   to digestion. The filter was then rinsed into borosilicate glass test tubes with 10ml hydrogen peroxide

445   (H_2O_2) 30%w/w, capped with glass stoppers, and placed in a static heat block (thermomix) at 55°C for

446   7 days (no agitation). On day 8 a further 5ml of H_2O_2 30%w/w was added to each sample and the

447   sample was left for a further 7 days. H_2O_2 was chosen as the digestion medium as used by previous

448   studies [7,30,38,39] however given the low usage temperature of some plastics (PS=70°C PVC=60°C)[40] and

449   risk of glassing or melting at elevated temperatures, the temperature was purposefully maintained

450   below 60°C to ensure the methodology did not affect the characterisation or result in loss of

451   material.

452   On day 14 the sample was filtered onto a 0.45μm PTFE 47mm dia. filter membrane, rinsed with

453   250ml MilliQ (18 MΩ.cm) water and dried with ethanol (96%.vol). Filtered material was then rinsed

454   into density separation glassware with zinc chloride (technipur $ZnChl_2$) at 1.6g/ml density. This was

455   gently agitated (60rpm) for 7 days at room temperature (Edmund Buhler KS-15 shaker). Settled

456   material was drained away with the sediment removal valve and remaining sample filtered onto

457   0.2μm, 25mm dia. aluminium oxide filters (Andodisc[TM] 25). Glassware was triple rinsed onto the filter

458   with pH4 buffer. The filter was then rinsed with 250ml MilliQ water and vacuum dried with ethanol.

459   The resulting filter was then examined and photographed again to look for changes in either the

460   number of particles or particle character. Whilst it is difficult to quantify particles pre-digestion (due

461   to excessive organic/inorganic material) many of the particles photographed previously were

462   identifiable and any visible change in the material was noted, thus we are confident that the

463   protocols were sufficiently gentle to ensure minimal losses of material.

464   **Blank test**

465   Two sets of laboratory blanks were created in support of this sample preparation process. Two MilliQ

466   samples of 1L, instead of field sample material, were put through the full digestion and zinc chloride

467   separation process, resulting in two full-process blanks (following in detail the process outlined for

468   the sample preparation).

469   A further two laboratory blanks (MilliQ water samples) underwent the digestion process but were

470   filtered onto the Anodisc[TM] 25 filters without zinc chloride separation. The purpose of these blanks

471   was to help quantify the possible MP contamination resulting from the sampling and sample

472   preparation process.

473   Field blanks were also collected from each collector. Sample collection containers (glass) were taken

474   out on site, connected to and opened at the sample location and then returned to the laboratory.

475   These 'empty' glass containers were then thoroughly rinsed with MilliQ water and the resulting

476   water processed without zinc chloride separation, following the preparation described above.

477   The blank test resulted in a total of 6 blank samples, 2 from the complete preparation and ZnCl2

478   process and 4 without ZnCl2 separation (n = 6). The blank filters identified on average 3 (±1) fibres, 1

479   (±1) film and 8 (±1) fragments per filter.

480   **Visual and ImageJ/FIJI particle inspection and count**

481   All filters were visually inspected under a stereo microscope for MP particles using the identification

482   criteria published by Hidalgo-Ruz (2012), Löder and Gerdts (2015), Norén (2007) [27,28,41]. It is noted

483   that using visual identification alone is not recommended for MP < 500µm, a second technique (FTIR,

484   Raman) is recommended to confirm for small particles [27,28,41,42]. Plastic particulates are visually

485   identified by their shape and colour. Plastics must have no biogenic (cellular) structure; fibres are

486   expected to have a relatively even or consistent thickness along the fibre length and illustrate three

487   dimensional bending; fragments and films are expected to have relatively homogeneous colouring

488   and illustrate a level of transparency or clarity [28,41]. Aged plastic, such as expected in environmental

489   samples, are described by Hidalgo-Ruz (2012)[27] as presenting embrittled and weathered surfaces, to

490   have irregular shapes with broken and sharp edges. Weathered plastics may also show pitting. Colour

491   is also a plastic identifier [27,41], ranging from transparent and variations of white to bright orange,

492   blues, greens and purples through to black. It is noted that biogenic material becomes bleached

493   during the sample preparation process (H_2O_2 digestion) making plastic particulates with colour highly

494   visible and differentiated from residual (post-digestion) biogenic material.

495   An initial, indicative fragment, fibre and film count was visually undertaken for each sample using an

496   Olympus SZX10stereo microscope. Three locations of 13mm^2 were randomly selected and

497   investigated on each filter (two filters per sample) (random selection to minimise bias) (Peeken

498   2018). Following the visual identification methodology, a count of plastic fragments, fibres and films

499   was undertaken (n = 6 inspected areas for each sample, total of 254 MP identified). Identification

500   was conservative with a focus on obvious coloured particulates, resulting in a possible under

501   estimation overall due to limited count or testing of white and non-transparent materials.

502 All filters were then photographed using a Leica DM6000M confocal microscope with a Marzhauser

503 Scan 130/85-4mm X-Y motorised stage. Photographs were manually focused for each frame using a

504 x10 lens. Filters were photographed using the automated mosaic software (Leica proprietary

505 software) and automatically stitched to provide a multistep mosaic image for each filter. The visual

506 count was repeated on the photographs and completed using the software ImageJ. Three 13mm^2

507 photographed areas of each filter were imported into ImageJ. Particle counts were undertaken using

508 the protocol defined and used by Erni-Cassola et al. (2017)[30] (ImageJ code provided in Erni-Cassola et

509 al (2017)[30] supplementary material doi: 10.1021/acs.est.7b04512). A second count was undertaken

510 following the same method using a larger area (6 x 58mm^2), providing a visual/ImageJ MP count for

511 50% of the Anodisc^{TM} 25 filter surface. All identified particles (n = 1147) were sized using ImageJ (as

512 completed in Isobe et al. 2015, Imhof et al. 2016[43,44]), providing a length, width and area appropriate

513 for particle size distribution analysis.

514 **Raman set up and analysis**

515 Confirmation of plastic presence and type was achieved by μRaman (Horiba Scientific Xplora Plus, 50-

516 3200cm^{-1} with a 1.5cm^{-1} resolution, confocal imaging accuracy 0.5 μm) confocal microscope with

517 motorised X-Y stage. μRaman spectroscopy has been used in previous studies to confirm visual and

518 Nile Red fluorescence assisted microplastic quantification in environmental samples[30,41,45–48] and has

519 been shown to be effective in microplastic characterisation down to 1 μm[19]. Three areas of each filter

520 (6 x 13mm^2) were randomly selected and analysed for total plastic presence using the 785nm laser

521 (spatial resolution of 1 μm) and 200-2000cm^{-1} Raman shift range. Spectra were collected using an

522 acquisition time of 15 seconds and 10 accumulations, maximum of 25% power (filter) (general

523 settings: grating of 1200gr_mm and 50μm split, modified to achieve effective spectra results as

524 necessary during analysis). Laser power setting were tested on plastic particles to establish the

525 strength necessary for effective spectra imaging with minimal particulate damage. Laser power of

526 25% resulted in no visible damage to the plastics and acceptable spectra delineation. Laser power of

527   50% and 100% result in damage (burning or melting) of the plastic as shown in the Supplementary

528   Note 4 – Images of Raman laser impact on plastic.

529   Each suspected plastic particle was analysed individually, resulting in a dataset of Raman shift

530   spectra's (n = 245 particulate). Each potential identified MP was analysed twice (at two unique

531   locations on the particle) to confirm the Raman spectra. Where the spectra were unclear or not

532   definitive, a third analysis was undertaken. Samples illustrating three unclear spectra were defined as

533   'not plastic'. The blank filters were tested to quantify the level of contamination (through sample

534   processing and analysis). A new Anodisc^{TM} 25 filter was also analysed to confirm the background filter

535   spectra. The μRaman spectral analysis provided conformation of visual identification, supporting the

536   extrapolation of visual counts to consider spatial and temporal trends.

537   **Raman Spectra analysis**

538   The open source Spectragryph software and databases[49] were used to analyse μRaman spectral

539   results. Individual evaluation of each spectrum was completed, similar to methods of spectra analysis

540   followed in [45,50,51] in conjunction with [52] which provides a clear definition of chemical and bond

541   spectra peaks.

542   **Statistical analysis**

543   Visual and ImageJ MP counts of all filters were confirmed using μRaman spectrography (11% of the

544   filters were analysed using μRaman, 50% of the filters were inspected visually and with ImageJ). The

545   μRaman confirmed count of MP ($\#/mm^2$) was extrapolated to provide an indication of the quantity of

546   MP per filter and therefore per sample. It is acknowledged that extrapolation from subsampled

547   filters does not provide a definitive MP count and ideally all MP particulates would be counted and

548   confirmed with μRaman analysis. Due to analysis constraints complete filter analysis was not

549   possible.

550 The calculation of MP per m^2/month (31 days) was calculated through a simple sum of sample area

551 MP counts, scaling using known filter and collector areas and known monitoring period durations.

552 The calculations followed the following simple equations.

$$\bar{X} = \frac{(\sum X_{1-n})}{n}$$

553   Eqn. 1

554 $\bar{X}$ = the average MP count for a sample area (13mm^2)

555 $X_{1, 2, 3}$ = the MP count for a sample area 1, 2, 3 etc. (sample area = 13mm^2)

556 n = sample area number (6 sample areas were investigated for each sample period)

$$\mu P = \left(\bar{X} \times \frac{Y}{y} \right) - \varepsilon$$

557   Eqn. 2

558 μP = total MP count per filter

559 y = sample area (13mm^2 or 0.000013m^2)

560 Y = total filter area (346 mm^2 or 0.0003m^2)

561 ε = sampling error, the number of MP particulates found on the blank samples

562

$$MP = \left(\mu P \times \frac{1}{a} \right) /d$$

563   Eqn. 3

564 MP = MP count per m^2 / day

565 a = sample area of the atmospheric collector (m^2)

566 d = duration of the sampling period (days)

567 The quantity of MP/filter is accepted to be representative of the atmospheric deposition for the

568 monitoring period relative to the collection area (Palmex collector = 0.014m^2, NILU collector =

569 0.03m^2). Provision of MP quantity/m^2 has been previously published and accepted as a method

570 supporting comparison of multiple studies results[8]. Therefore, the results per monitoring period

571 were normalised for 1 day time period (for comparison to Dris et al.[11] and Cai et al.[12]) and 1 metre

572 square area using the known collector surface areas. The two collectors provide replicate samples for

573   each sample period and therefore were treated as such. Thus, two independent samples were

574   collected for each sample period, providing 2 Anodisc^{TM} 25 filters, with a total of 6 randomly selected

575   areas analysed for MP resulting a per monitoring period n= 6.

576   Statistical analysis of the MP counts and characteristics has been purposefully kept to a minimum

577   due to the dataset duration (5 monitoring periods) and the single site case study constraints (it is not

578   considered appropriate to generalise from a single case study), the study is presented as a first

579   indication and presentation of remote MP presence only). Simple correlation analysis between

580   particle counts and meteorological data was completed using R Studio (R version 3.4.1) software and

581   standard significance (p-value), Pearson and Spearman correlation tests used appropriate to the data

582   (CRAN packages hydroGOF, Hmisc, Performance Analytics and subsidiaries).

583   **Bias**

584   Use of a non-automated system in particle counting and analysis will induce a level of human bias in

585   the results. To reduce the potential human bias in the results due to lack of automation, random

586   sampling has been employed on all filter counting and µRaman analysis site selection. MP visual,

587   ImageJ and µRaman analysis has been undertaken in triplicate on all filters to further limit bias and

588   uncertainty in the results. MP identification was completed following an identification protocol that

589   was consistently employed on all areas analysed. The identification protocol was conservative, any

590   particles that did not meet visual identification protocol as described by Hidalgo-Ruz et al.[27] and

591   Norén [28] and or did not provide a clear Raman plastic signature were discounted from the analysis to

592   limit mis-identification and bias.

593   **Local transport trajectory and source area assessment**

594   The recorded wind, rain and snow meteorological data was used to support a local MP transport

595   assessment and to help consider potential source and trajectories of MP relative to the field site. The

596   simple numerical assessment of distance and transport duration of MP particles relative to rainfall

597   events, snowfall events and wind occurrences (events) were calculated using the known field site

598 elevation, upper elevation of MP entrainment[37], wind speed and assumed settling velocity[36] (based

599 on 25μm dust particle). Once elevated, it was assumed that no further meteorological updraft or

600 conveyance assistance (other than recorded horizontal wind speed and direction) influenced the MP

601 (to provide a simplified assessment of possible MP transport).

602 $$distance \ = \ back - trajectory \ duration \Big/ wind \ speed \qquad \text{Eqn. 4}$$

603 *distance* = potential horizontal trajectory of MP (m)

604 *back-trajectory duration* = the duration MP is airborne (sec); calculated as maximum elevation (600m

605 a.g.l)[37]/ settling velocity (0.1 m/s)[36]

606 *wind speed* = maximum recorded wind speed (at the meteorological station) during each rain, snow

607 or wind event (m/s)

608 The wind direction recorded for the rain, snow and wind events were used in conjunction with the

609 calculated horizontal transport distances to create event specific wind rose maps to spatially

610 illustrate the local MP trajectories. It is acknowledged that this is a highly simplified assessment of

611 potential horizontal transport trajectories and does not take into account the complex atmospheric

612 dynamics of mountain terrain or atmospheric mixing. However, it does provide a first simplified

613 assessment of local MP transport.

614 **HYSPLIT4 analysis**

615 The open source modelling software HYSPLIT[53,54] was used to model the back trajectory of air parcel

616 movement from the field site during the five monitoring periods. HYSPLIT version 4 (HYSPLIT4) was

617 used to download and model global wind/atmospheric meteorology data provided by NOAA (Global

618 Data Assimilation System data) (similarly used in[55–57]). Each rainfall (n=165), snowfall (n=186) and

619 wind event >2m/s (n=197) were individually modelled with the back-trajectory duration defined

620 above (Eqn. 4). The multiple individual trajectories were then collated to create a frequency chart of

621   trajectory potentials across the local area. The source point (deposition location in a back-trajectory

622   model) was set to 43N 1E 100m a.g.l.
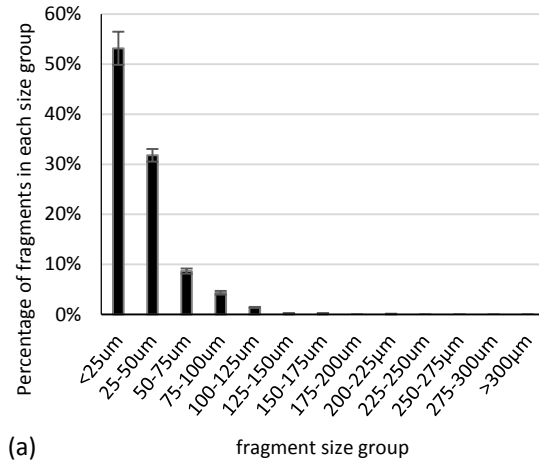
623   **Methodology References**

624   38.   Digka, N., Tsangaris, C., Kaberi, H., Adamopoulou, A. & Zeri, C. Microplastic Abundance and

625   Polymer Types in a Mediterranean Environment. in *Proceedings of the International*

626   *Conference on Microplastic Pollution in the Mediterranean Sea* (eds. Cocca, M. et al.) 17–24

627   (Springer Water. Springer, Cham, 2018). doi:10.1007/978-3-319-71279-6

628   39.   Wang, W., Ndungu, A. W., Li, Z. & Wang, J. Microplastics pollution in inland freshwaters of

629   China: A case study in urban surface waters of Wuhan, China. *Sci. Total Environ.* **575**, 1369–

630   1374 (2017).

631   40.   Klein, R. Material Properties of Plastics. in *Laser Welding of Plastics: Materials, Processes and*

632   *Industrial Applications* 3–69 (John Wiley & Sons, 2012). doi:10.1002/9783527636969

633   41.   Löder, M. & Gerdts, G. Methodology used for the detection and identification of microplastics

634   – a critical appraisal. in *Marine Anthropogenic Litter* (eds. Bergmann, M., Gutow, L. & Klages,

635   M.) (Springer, Cham, 2015). doi:10.1007/978-3-319-16510-3_8

636   42.   Shim, W. J., Hong, S. H. & Eo, S. E. Identification methods in microplastic analysis: a review.

637   *Anal. Methods* **9**, 1384–1391 (2017).

638   43.   Isobe, A., Uchida, K., Tokai, T. & Iwasaki, S. East Asian seas: A hot spot of pelagic microplastics.

639   *Mar. Pollut. Bull.* **101**, 618–623 (2015).

640   44.   Imhof, H. K. *et al.* Pigments and plastic in limnetic ecosystems: A qualitative and quantitative

641   study on microparticles of different size classes. *Water Res.* **98**, 64–74 (2016).

642   45.   Lenz, R., Enders, K., Stedmon, C. A., MacKenzie, D. M. A. & Nielsen, T. G. A critical assessment

643   of visual identification of marine microplastic using Raman spectroscopy for analysis

644   improvement. *Mar. Pollut. Bull.* **100**, 82–91 (2015).

645   46. Enders, K., Lenz, R., Stedmon, C. A. & Nielsen, T. G. Abundance, size and polymer composition

646   of marine microplastics ≥10μm in the Atlantic Ocean and their modelled vertical distribution.

647   *Mar. Pollut. Bull.* **100**, 70–81 (2015).

648   47. Käppler, A. *et al.* Analysis of environmental microplastics by vibrational microspectroscopy:

649   FTIR, Raman or both? *Anal Bioanal Chem* **408**, 8377–8391 (2016).

650   48. Song, Y. K. *et al.* A comparison of microscopic and spectroscopic identification methods for

651   analysis of microplastics in environmental samples. *Mar. Pollut. Bull.* **93**, 202–209 (2015).

652   49. Menges, F. Spectragryph – optical imaging software. (2016). Available at:

653   https://www.effemm2.de/spectragryph/.

654   50. Khashaba, P. Y., Ali, H. R. H. & El-Wekil, M. M. A rapid Fourier transform infrared

655   spectroscopic method for analysis of certain proton pump inhibitors in binary and ternary

656   mixtures. *Spectrochim. Acta Part A Mol. Biomol. Spectrosc.* **190**, 10–14 (2018).

657   51. Ševčík, R. & Mácová, P. Localized quantification of anhydrous calcium carbonate polymorphs

658   using micro-Raman spectroscopy. *Vib. Spectrosc.* **95**, 1–6 (2018).

659   52. Lagaron, J. M., Dixon, N. M., Reed, W., Pastor, J. M. & Kip, B. J. Morphological characterisation

660   of the crystalline structure of cold-drawn HDPE used as a model material for the

661   environmental stress cracking (ESC) phenomenon. *Polymer (Guildf).* **40**, 2569–2586 (1999).

662   53. Draxler, R. R. & Hess, G, D. Hysplit4 modeling system. (2018).

663   54. Stein, A. *et al.* NOAA's HYSPLIT atmospheric transport and dispersion modeling system. *Bull.*

664   *Am. Meteorol. Soc.* **96**, 2059–2077 (2015).

665   55. Su, L., Yuan, Z., Fung, J. C. H. & Lau, A. K. H. A comparison of HYSPLIT backward trajectories

666   generated from two GDAS datasets. *Sci. Total Environ.* **506–507**, 527–537 (2015).

667   56.   Ashrafi, K., Shafiepour-Motlagh, M., Aslemand, A. & Ghader, S. Dust storm simulation over

668   Iran using HYSPLIT. *J. Environ. Heal. Sci. Eng.* **12**, 9 (2014).

669   57.   Reche, I., D'Orta, G., Mladenov, N., Winget, D. M. & Suttle, C. A. Deposition rates of viruses

670   and bacteria above the atmospheric boundary layer. *ISME J.* (2018). doi:10.1038/s41396-017-
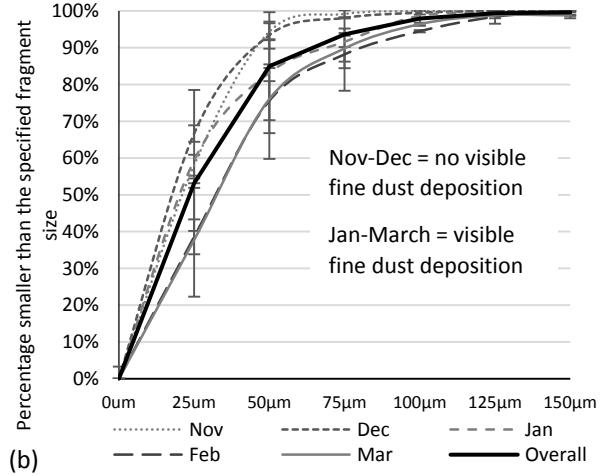
671   0042-4

672

(b) Microplastic particle count

(d)

(e)
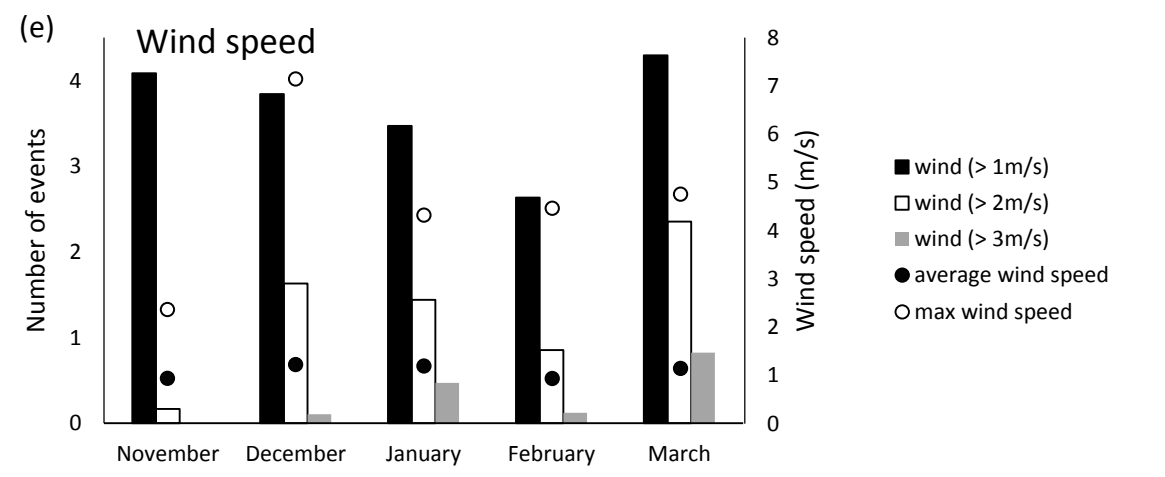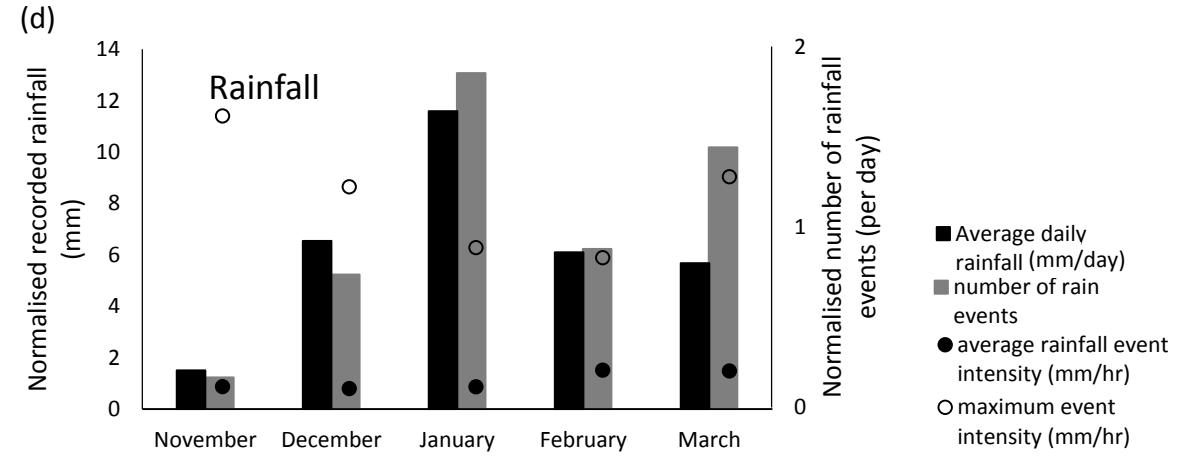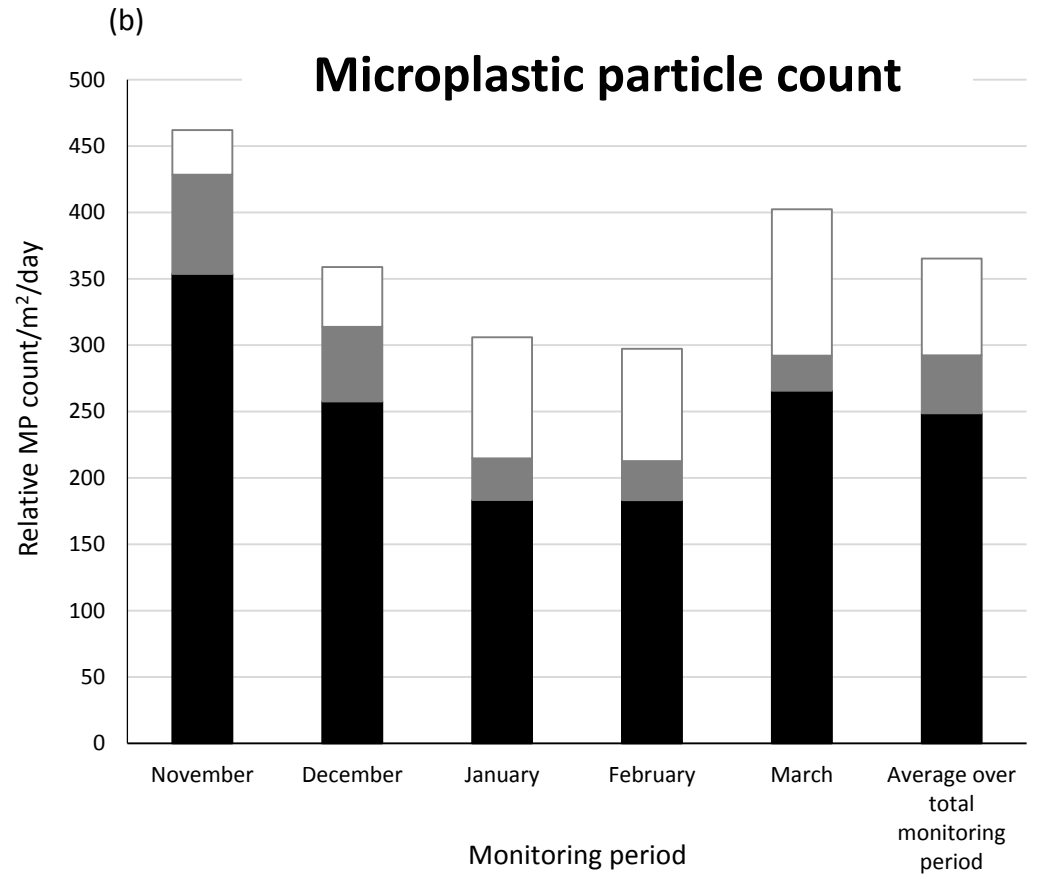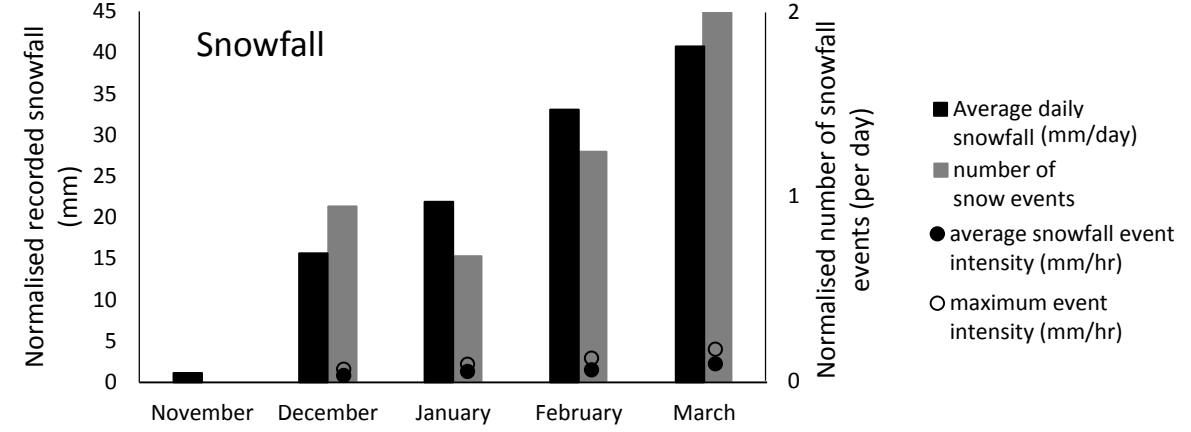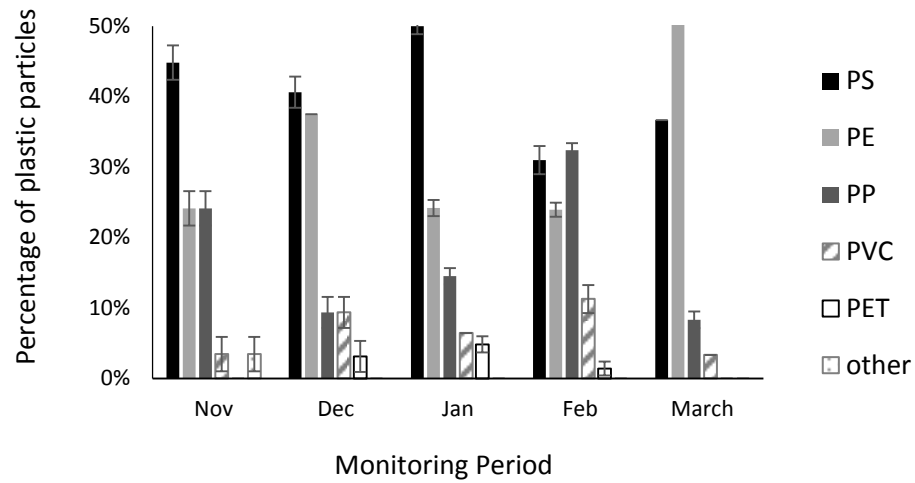
(a) Particle size distribution of fragments in the atmospheric deposition samples

(b) Particle size distribution by sample period

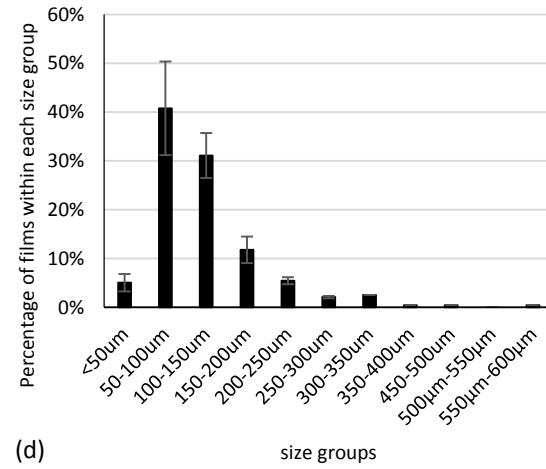Nov-Dec = no visible fine dust deposition

Jan-March = visible fine dust deposition

(c) Fibre lengths
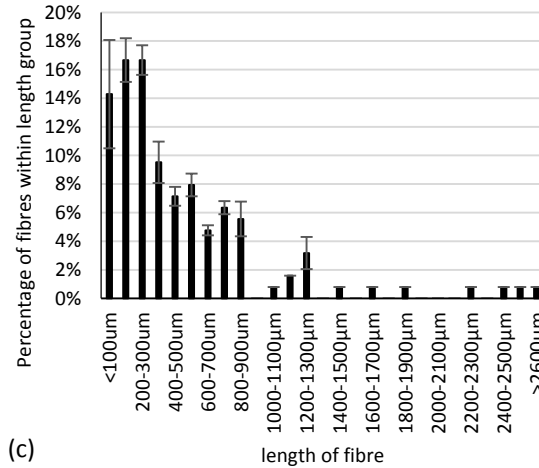
(d) Size of films in deposition

(a) MP potential transport trajectories Snow and Rain events — Taracon-sur-Ariège

Population
- <100
- 100-200
- 200-300
- 300-400
- 400-500
- 500-600
- > 600

(b) MP potential transport trajectories Wind events >2m/s — Foix, Tarascon-sur-Ariège

Population
- <500
- 500-1000
- 1000-2000
- 2000-4000
- 4000-6000
- 6000-8000
- >8000

(c) Wind events — Foix, Tarascon-sur-Ariège

Population
- <5000
- 5000-10,000
- 10,000-15,000
- 15,000-20,000
- 20,000-25,000
- 25,000-30,000
- > 30,000

(d) Rainfall events

(e) Snowfall events

- 0.1% trajectory frequency
- 1% trajectory frequency
- 10% trajectory frequency
- ▲ Bernadouze Field Site